LEVEL II

AFGL-TR-80-0209
AIR FORCE SURVEYS IN GEOPHYSICS, NO. 428

Horizontal Scale Variations in Satellite Estimates of Weather Erosion Parameters for Reentry Systems

JAMES T. BUNTING
CHANKEY N. TOUART

26 June 1980

METEOROLOGY DIVISION PROJECT 6670
AIR FORCE GEOPHYSICS LABORATORY
HANSCOM AFB, MASSACHUSETTS 01731

AIR FORCE SYSTEMS COMMAND, USAF

This report has been reviewed by the ESD Information Office (OI) and is releasable to the National Technical Information Service (NTIS).

This technical report has been reviewed and
is approved for publication.

FOR THE COMMANDER

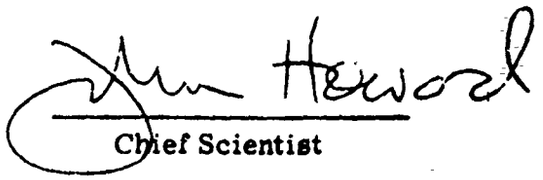

Chief Scientist

Qualified requestors may obtain additional copies from the Defense Technical Information Center. All others should apply to the National Technical Information Service.

(9) Air Force surveys in geophysics

Unclassified

SECURITY CLASSIFICATION OF THIS PAGE (When Data Entered)

REPORT DOCUMENTATION PAGE	READ INSTRUCTIONS BEFORE COMPLETING FORM
AFGL-TR-80-0209	2. GOVT ACCESSION NO. AD-A092 447 / 3. RECIPIENT'S CATALOG NUMBER
(6) HORIZONTAL SCALE VARIATIONS IN SATELLITE ESTIMATES OF WEATHER EROSION PARAMETERS FOR REENTRY SYSTEMS.	5. TYPE OF REPORT & PERIOD COVERED: Scientific. Interim.
	6. PERFORMING ORG. REPORT NUMBER: AFSG No. 428
7. AUTHOR(s): (10) James T. Bunting, Chankey N. Touart (12) 30	8. CONTRACT OR GRANT NUMBER(s)
9. PERFORMING ORGANIZATION NAME AND ADDRESS: Air Force Geophysics Laboratory (LYU), Hanscom AFB, Massachusetts 01731 (16)	10. PROGRAM ELEMENT, PROJECT, TASK AREA & WORK UNIT NUMBERS: 62101F, 667Ø1201 (17) 42
11. CONTROLLING OFFICE NAME AND ADDRESS: Air Force Geophysics Laboratory (LYU), Hanscom AFB, Massachusetts 01731 (11)	12. REPORT DATE: 26 June 1980; 13. NUMBER OF PAGES: 29
(14) AFGL-TR-80-0209, AFGL-AFSG-428 — 14. MONITORING AGENCY NAME & ADDRESS (if different from Controlling Office)	15. SECURITY CLASS. (of this report): Unclassified; 15a. DECLASSIFICATION/DOWNGRADING SCHEDULE

16. DISTRIBUTION STATEMENT (of this Report)

Approved for public release; distribution unlimited.

17. DISTRIBUTION STATEMENT (of the abstract entered in Block 20, if different from Report)

18. SUPPLEMENTARY NOTES

19. KEY WORDS (Continue on reverse side if necessary and identify by block number)

Weather satellites	Environmental severity index
Infrared sensors	Liquid water content
Visible sensors	Precipitation
Horizontal resolution	Clouds
Hydrometeors	

20. ABSTRACT (Continue on reverse side if necessary and identify by block number)

A weather erosion parameter known as the Environmental Severity Index (ESI) has been estimated using infrared and visible data from satellites. Cloud sampling requirements limited the original prediction equations to satellite data averaged over a horizontal scale of 70 km. Further experiments have demonstrated great utility for satellite estimates on a scale of 10 km and also revealed some systematic differences between the coarse and the fine scale estimates. The ESI averages 1 percent to 10 percent higher for the fine scale estimates and high values of ESI are observed more frequently.

DD FORM 1 JAN 73 1473 EDITION OF 1 NOV 65 IS OBSOLETE

Unclassified

SECURITY CLASSIFICATION OF THIS PAGE (When Data Entered)

409578 ALK

Contents

Illustrations

Illustrations

Tables

Horizontal Scale Variations in Satellite Estimates of Weather Erosion Parameters for Reentry Systems

1. INTRODUCTION

1.1 Previous Studies

The Meteorology Division of the Air Force Geophysics Laboratory (AFGL) conducted a lengthy experiment to provide satellite estimates of weather erosion parameters for reentry systems.[1] The term "weather erosion" refers to material erosion of surfaces on high-velocity reentry vehicles impacted by precipitation and cloud particles. The work supported the Advanced Ballistic Reentry Systems (ABRES) program of weather erosion studies.

The AFGL experiment was a series of simultaneous measurements of clouds and precipitation by research aircraft and weather satellites. The aircraft instruments estimated particle mass densities at all altitudes at which clouds were present and the aircraft could safely operate. The weather satellites sensed infrared (IR) radiation emitted by the upper regions of the clouds and also visible radiation reflected by clouds during daytime. The aircraft measurements of particle mass density were reduced to weather erosion parameters using engineering models relating hydrometeor data to reentry vehicle erosion and accuracy. Using a statistical approach, nonlinear equations were derived to estimate weather erosion parameters

(Received for publication 26 June 1980)

1. Conover, J.H., and Bunting, J.T. (1977) Estimates From Satellites of Weather Erosion Parameters for Reentry Systems, AFGL-TR-77-0260, AD A053654.

from the simultaneous satellite measurements of IR and visible radiation. The resulting equations were applied extensively to produce climatologies of weather erosion potential over Europe, Asia, and test ranges such as Kwajalein.

The horizontal scale of satellite-based weather erosion estimates has been a subject of concern since the beginning of the satellite correlation studies and the choice of scale reflects tradeoffs between available satellite data and the requirements of reentry design and testing. The AFGL experiment was designed to provide erosion parameter estimates averaged over areas of about 70 × 70 km. This size is approximately the same as the horizontal resolution of a satellite IR sounder with data that was archived and well documented.[1] During the course of the experiment, we found that the IR sounder data and a simple radiation model provided good estimates of cirrus altitude, IR transmissivity, and the Environmental Severity Index (ESIp, defined in Section 1.2 of this report) in the range of 0 to 1. Later, the program sponsors found that they had a greater need for erosion climatologies for ESIp of 2 or greater and we determined that the higher values of ESIp were better estimated from a combination of visible and IR data available from the satellite imagery. Since the satellite imagery data was available at a finer resolution of 10 × 10 km, we were faced with the decision of retaining the 70 × 70 km horizontal scale and averaging the finer resolution data to that scale or else revising the experiment to examine a finer scale. The larger scale of 70 × 70 km was retained for the following reasons: (1) More aircraft flights and lengthy data reduction would have been required to repeat the experiment on a finer scale. (2) The larger scale was convenient since aircraft could ascend or descend in a wide diameter spiral. (3) The earth location of the satellite data was in doubt by as much as 20 km for some of the archived data, and some uncertainty remained after adjustments. A larger horizontal area increased confidence that the aircraft was sampling clouds within the view of the satellite. (4) During the 30 to 60 min required for aircraft sampling, clouds could advect, grow, or dissipate, and averages over larger horizontal areas appeared to be less sensitive to these changes. (5) The archived NOAA satellite data tapes had some peculiar records and other noise which gave false alarms since IR data were excessively cold. This particular problem was greatly reduced with satellite data averaged over an array of tape records and data values within the records. (6) For climatological applications over areas as large as Eurasia, the finer resolution provides an unwieldy number of weather erosion estimates.

Unlike the development sample of satellite data, the physical interaction of a reentry vehicle colliding with hydrometeors represents a very small scale. Just how accurately the satellite estimates represent erosive weather at these smaller scales is the primary subject of this report. For a vehicle reentering at a nominal angle of 30° above the horizon at an area such as Kwajalein, where significant

weather may exist from the surface to 17 km, the vehicle may pass along a 34 km slant path of hydrometeors. The volume of weather eroding the vehicle would then be roughly 34 km times its diameter. The volume of influence would in general be smaller, depending primarily on the thickness and horizontal coverage of the clouds. When these numbers are compared to the 70 × 70 km of horizontal area of satellite data, the 34 km length compares reasonably well but the width of the reentry vehicle does not. A more appropriate area for satellite data might be aligned along the track of the vehicle with a length about twice the thickness of the clouds and a width as thin as the satellite data would permit.

The various satellites and scales of horizontal resolution are summarized in Table 1. These resolutions are rough approximations to sampling sizes on the earth's surface. A systems engineering discussion of resolution is beyond the scope of this report. Table 1 shows that the IR and visible data are not truly coincident since the fields of view for IR data tend to be larger than for visible data. The difference is greater in the GOES applications. For the polar orbiting NOAA/ITOS satellites the difference is less, but both IR and visible data were archived at the same scale in hemispheric maps. The archive resolution of 10 × 10 km is larger than the sensor resolution except for IR data at high viewing angles.

Table 1. Scales of Satellite Data Used in Erosion Studies

Satellite	Sensor Resolution IR	Sensor Resolution Visible	Archive Resolution (Same for IR & Visible)
NOAA/ITOS			
At Subpoint	6 × 6 km	3 × 3 km	
At Max. Viewing Angle	12 × 12 km	6 × 6 km	
Algorithm Development			70 × 70 km*
Climatology Applications			50 × 50 km*
Special Applications			10 × 10 km
GOES			
At Subpoint	8 × 8 km	1 × 1 km	(Archive not used for GOES)
At Kwajalein Range (GOES WEST)	8 × 15 km	1 × 15 km*	
At Wallops Range (GOES EAST)	10 × 8 km	1 × 8 km*	
Special Application at Kwajalein	40 × 75 km*	5 × 75 km*	

*Averaged Data

In previous studies, considerable experience was gained from practical applications of weather erosion estimates to finer satellite data for both polar orbiting and geostationary satellites. These applications were made despite the fact that the algorithms are nonlinear* so that erosion estimates can increase greatly when the equations are applied to smaller areas with colder IR and brighter visible measurements. The fine scale estimates were verified with limited samples of radar and aircraft data. Fine scale estimates were also used to forecast weather erosion potential over Kwajalein. The satellite estimates did not "blow up" by providing obviously bad answers when satellite data well outside the range of the development sample was used. In fact, the fine scale estimates appeared to be more useful than the original 70 × 70 km estimates for highly convective weather regimes such as Kwajalein.

1.2 Approach

In this report, the Environmental Severity Index for precipitation particles (ESIp) is estimated from various scales of satellite data and comparison statistics are generated. The ESIp is defined as

$$\text{ESIp} = \int_0^\infty \rho \, H dH \; (\text{g km}^2 \text{ m}^{-3}) \tag{1}$$

where ρ is the density (g m^{-3}) of hydrometeors larger than 50 μm in diameter, H is the altitude (km) above the ground, and the integral is taken over all altitudes. The ESIp is approximately linearly related to the depth of material recession on the nosetip of a reentry vehicle, although the constants of relation vary with the design of the vehicle. In all cases, the ESIp was estimated from satellite data using the equation

$$\text{ESIp} = \frac{746.249}{(\overline{IR} - 148.800)} + \frac{177.500}{(288.700 - \overline{B}_N)} - 7.395 . \tag{2}$$

When Eq. (2) yields an estimate of ESIp less than zero, the ESIp is set at zero since ESIp values less than zero are not defined by Eq. (1). The derivation of Eq. (2) and its accuracy have been discussed at length.[1] In this study, it is used for all scales of satellite data. The quantity $\overline{IR}$ is the average 10 to 12 μm infrared temperature (degrees Kelvin) sensed by the satellite. For fine scale estimates, only one IR measurement is available and it is used as $\overline{IR}$. The quantity $\overline{B}_N$, the normalized

*More specifically, satellite data are linearly averaged over an area. The averages are put in nonlinear equations to estimate weather erosion parameters.

mean visible brightness, is the average reflected sunlight measured by the satellite in the spectral bandwidth of 0.5 to 0.7 μm. $\overline{B}_N$ has the same units (fL $\times$ 40) used for archives of the NOAA/ITOS satellites. In the archives, visible data values range from 0 to 254 and these numbers are approximately equivalent to cloud reflectivities from 0 to 90 percent. All visible data used in Eq. (2) have been normalized for anisotropic reflection to estimate what the satellite would see if both the sun and the satellite were directly over the cloud.

Two separate data sets were used to compare satellite estimates over larger areas to estimates over small areas. These small areas are the unaveraged scales of IR satellite data shown in Table 1, and they are as close as we can approximate the very small scale of reentry erosion. The first set was GOES-West data near Kwajalein Atoll for 12 occasions in June, July, November, and December 1977. The second set was NOAA 2 data over 11 stations in Europe and Asia for the months of May, July, and October 1973. For both data sets, ESIp was calculated for the finest resolution of data and also for averages of data over 5 $\times$ 5 grids. These two scales of ESIp estimates are subsequently represented by ESI_1 and ESI_5. There are 25 values of ESI_1 for each ESI_5. The 25 values of R defined as ESI_1/ESI_5 were also calculated for each ESI_5. Frequency distributions of R, ESI_1, and ESI_5 along with discussion are given in Section 2. The second data set is also compared to ESIp estimates based on radiosonde, rainfall, and surface data at the 11 stations in Europe and Asia. Areas and numbers of cases for both data sets are given in Table 2.

Table 2. Comparison of ESIp Data Sources

	Kwajalein	Eurasia
Satellite	GOES-West	NOAA 2
Area for ESI_1	8 $\times$ 15 km	10 $\times$ 10 km
Area for ESI_5	40 $\times$ 75 km	50 $\times$ 50 km
Total Cases ESI_5	170	847
Number $ESI_5 > 0$	170	256
Number $ESI_5 \geq 2$	135	34

2. COMPARISONS OF EROSION PARAMETER ESTIMATES FOR DIFFERENT SCALES

2.1 Estimates Near Kwajalein

Satellite data were taken from printouts generated by the Man-computer Interactive Data Access System (McIDAS) at AFGL. The McIDAS was used to obtain IR and visible data from the GOES-West Satellite as an aid in forecasting for weather erosion tests at the Kwajalein Missile Range. Twelve occasions in June, July, November, and December 1977 were used. These occurred at various times of the morning (Kwajalein time) with the sun at least 15° above the horizon in order for visible data to be useful.

In the main, the printouts were 25 × 25 grids positioned over areas near Kwajalein that had been of operational interest at the time. A sample printout is shown in Figure 1 with latitudes, longitudes, and the Kwajalein Atoli superimposed. The 25 × 25 grids were subdivided into 25 5 × 5 grids. A total of 170 5 × 5 grids were selected and ESI_5, 25 ESI_1 values, and 25 R values were computed for each grid. Grids with ESI_5 equal to zero were ignored. The 5 × 5 grids were randomly positioned with respect to the clouds, but in the later stages of the data collection we did pick and choose among the 5 × 5 grids, so as to balance the data set with respect to ESI_5. The resulting data set overrepresents the higher values of ESIp and is not intended to represent a climatology of ESIp over Kwajalein. It did, however, provide significant numbers of high ESIp values for a reasonable effort.

After stratifying the data set according to value of ESI_5, cases were grouped into 11 classes of ESI_5 range according to Table 3. For each class, all values of R were combined and a mean value, standard deviation, frequency distribution, and a cumulative frequency distribution were derived. These are tabulated in Tables 3, 4, and 5. Figure 2 has plots of the cumulative frequencies.

Table 3 shows that $\overline{R}$ is greater than zero for all ranges of ESI_5 and this observation is expected due to the nonlinear relation of $\overline{IR}$ and $\overline{B_N}$ to ESIp in Eq. (2). If all 25 areas of a 5 × 5 array have the same values of IR and B_N then all 25 values of ESI_1 will be the same as ESI_5 and all values of R will equal 1.0 so that $\overline{R}$ will also equal 1.0. If, as is usually the case, the 25 areas have varying IR and B_N then the ESI_1 values for low IR and high B_N will be disproportionately greater than the ESI_1 values for high IR and low B_N and $\overline{R}$ will exceed 1.0.

Table 3 also shows that both $\overline{R}$ and σ_R tend to decrease as ESI_5 increases and these observations imply that the 5 × 5 arrays of IR and B_N are becoming more uniform as ESI_5 increases. There are two plausible meteorological explanations for this tendency. First, as the satellite observes cloud temperatures to decrease and visible brightnesses to increase so that the calculated ESI_5 increases, the

5×5 arrays may tend to have fewer clear areas and appear more uniform. Second, the highest values of ESI_5 over Kwajalein should correspond to satellite views of high, thick ice clouds such as the tops of thunderstorms or cirrus above the Intertropical Convergence Zone. In satellite IR and visible pictures these clouds appear more uniform than cumulus or cumulus congestus clouds at lower altitudes. For example, for ESIp of 8 or greater, putting reasonable values of $\overline{B}_N$ in Eq. (2) shows that the IR temperatures must be 220°K or less. These clouds would invariably have tops consisting of ice particles and be located within several kilometers or less from the Tropopause.

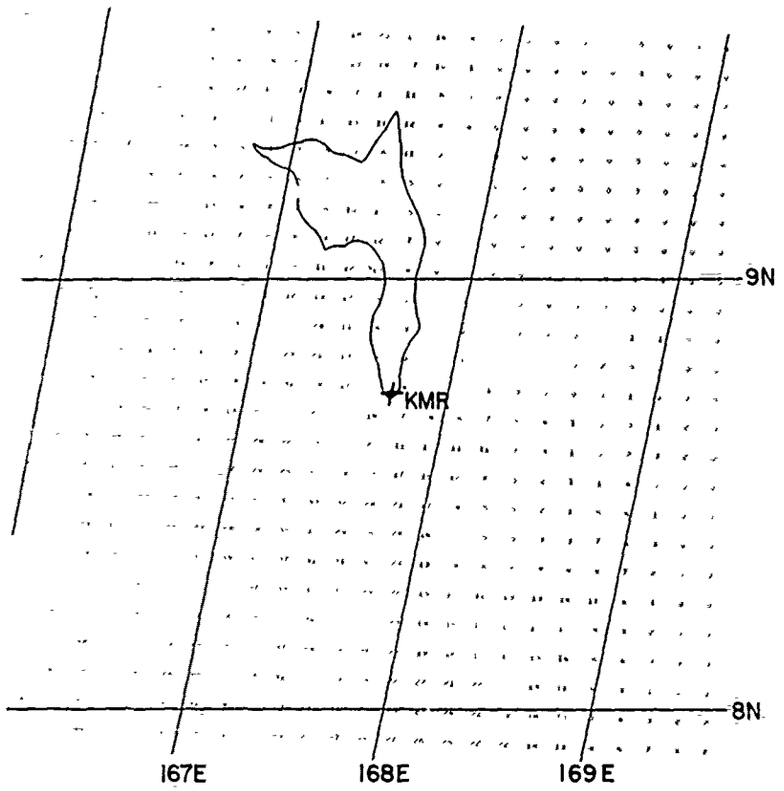

Figure 1. ESIp (in tenths) in the Vicinity of Kwajalein Atoll on 21 July 1977. ESIp estimates are based on IR and visible data from the GOES-West satellite

Table 3. Statistics of the Ratio, R, of ESI_1/ESI_5 Stratified According to the Value of ESI_5. N_5 is the number of ESI_5 within each range, $\overline{R}$ is the mean, and σ_R the standard deviation of the $25 \times N_5$ values of R

ESI_5 Range	N_5	$\overline{R}$	σ_R
< 1	19	1.922	4.1430
1-1.99	16	1.146	0.7753
2-2.99	19	1.076	0.5840
3-3.99	21	1.055	0.4421
4-4.99	19	1.042	0.3539
5-5.99	16	1.022	0.2232
6-6.99	12	1.021	0.1981
7-7.99	8	1.023	0.1994
8-8.99	16	1.011	0.1289
9-9.99	9	1.002	0.0962
≥ 10	15	1.005	0.1112

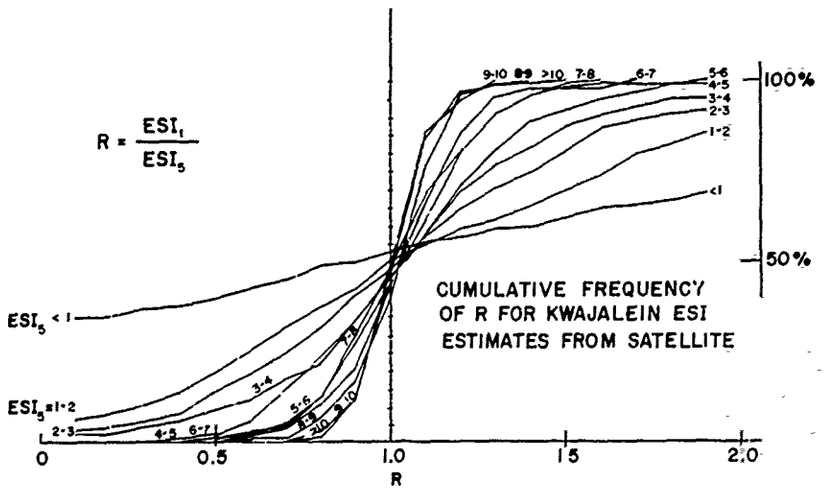

Figure 2. The Cumulative Frequency of the Ratio R Based on Satellite Estimates of ESIp Near Kwajalein. Curves are plotted for 11 classes of ESI_5 values

Table 4. The Frequency Distribution of R Values Stratified According to ESI_5

Frequency Distribution (%)											
	Range of ESI_5										
R	< 1	1-2	2-3	3-4	4-5	5-6	6-7	7-8	8-9	9-10	> 10
0 -0.1	33.7	5.6	2.5	1.7	0	0	0	0	0	0	0
0.1-0.2	1.5	2.8	1.7	0.8	0.2	0	0.3	0	0	0	0
0.2-0.3	2.1	2.8	2.1	1.1	0.2	0	0	0	0	0	0
0.3-0.4	0.8	3.1	2.1	1.9	0.6	0	0	0	0	0	0
0.4-0.5	2.1	5.6	5.3	3.2	1.3	0.8	0.7	0	0	0	0
0.5-0.6	2.5	6.1	4.8	3.6	3.8	1.0	1.7	2.0	0.5	0	0
0.6-0.7	2.1	5.9	6.3	5.3	8.8	2.3	1.7	2.5	0.8	0	0.3
0.7-0.8	4.0	5.6	6.7	4.8	8.8	8.0	6.7	7.0	5.5	1.3	2.6
0.8-0.9	1.3	5.4	9.3	12.0	10.1	16.8	9.7	16.5	10.3	10.7	9.1
0.9-1.0	3.2	7.2	7.4	12.0	11.4	18.8	22.0	16.0	22.5	36.9	33.3
1.0-1.1	2.3	4.6	9.1	11.2	13.1	21.0	24.7	18.0	37.5	37.3	39.7
1.1-1.2	1.7	4.3	7.6	12.6	12.8	12.5	18.7	17.0	19.5	8.4	11.7
1.2-1.3	1.7	2.8	6.1	6.7	10.3	10.3	9.7	10.5	2.0	5.3	1.9
1.3-1.4	2.3	4.6	4.4	5.1	7.4	4.5	1.7	5.0	1.3	0	0.5
1.4-1.5	2.5	3.3	5.9	5.7	3.6	2.3	0	3.5	0	0	0.5
1.5-1.6	1.9	4.3	5.7	3.2	2.7	1.3	1.0	1.0	0.3	0	0
1.6-1.7	1.5	5.9	1.7	2.1	2.1	0	0.3	0	0	0	0.3
1.7-1.8	0.8	3.1	2.1	1.5	1.3	0	0	0	0	0	0
1.8-1.9	2.1	2.8	1.5	0.4	0.6	0.3	0	0	0	0	0
≥ 1.9	30.9	14.1	7.8	5.0	0.8	0.5	0.3	0	0	0	0

Table 5. The Cumulative Frequency Distribution of R Values Stratified According to ESI_5

	Cumulative Frequency (%) Range of ESI_5										
R	< 1	1-2	2-3	3-4	4-5	5-6	6-7	7-8	8-9	9-10	> 10
< 0.1	34	6	3	2	0	0	0	0	0	0	0
< 0.2	35	8	4	2	0	0	0	0	0	0	0
< 0.3	37	11	6	4	0	0	0	0	0	0	0
< 0.4	38	14	8	6	1	0	0	0	0	0	0
< 0.5	40	20	14	9	2	1	1	0	0	0	0
< 0.6	43	26	19	12	6	2	3	2	1	0	0
< 0.7	45	32	25	18	15	4	4	5	1	0	0
< 0.8	49	38	32	22	24	12	11	12	7	1	3
< 0.9	50	43	41	34	34	29	21	28	17	12	12
< 1.0	53	50	48	46	45	48	43	44	40	49	45
< 1.1	56	55	57	58	58	69	67	62	77	86	85
< 1.2	57	59	65	70	71	81	86	80	97	95	97
< 1.3	59	62	71	77	81	91	96	91	99	100	99
< 1.4	60	66	75	82	89	96	98	96	100	100	99
< 1.5	63	70	81	88	92	98	98	99	100	100	100
< 1.6	65	74	87	91	95	99	98	100	100	100	100
< 1.7	66	80	89	93	97	99	100	100	100	100	100
< 1.8	67	83	91	95	99	99	100	100	100	100	100
< 1.9	69	86	92	95	99	100	100	100	100	100	100

2.2 Estimates in Europe and Asia

Satellite data were taken from the Northern Hemisphere archives of the NOAA 2 satellite over 11 stations in Europe and Asia for the months of May, July, and October 1973. At the rate of one satellite picture per station per day, a total of 1023 cases were possible. As listed in Table 2, only 847 cases were obtained due to incomplete satellite archives. Of these, 30 percent had ESI_5 greater than 0 and only 4 percent had ESI_5 greater than 2. These figures are climatically representative of summer weather at high latitudes of Eurasia during morning hours. They contrast greatly with the Table 2 figures for Kwajalein which are not intended to be climatically representative.

The 11 stations are identified in Table 6 and Figure 3. An ESI_5 value and 25 values of ESI_1 and R were computed for a 50 × 50 km area over each station. In the absence of special corrections the earth location of the archived data can be in error by 20 to 30 km so the 50 × 50 km areas are not always centered over the stations.

2.2.1 DISTRIBUTIONS OF R

Tables 7 and 8 have frequency and cumulative frequency distributions of R. The tables are not broken down so finely as Tables 4 and 5 since the Eurasian data sample had fewer high values of ESI_5. Only two ranges of ESI_5 values were considered, in the first case all values greater than 0 and in the second case all values greater than or equal to 2. The threshold of 2 was chosen based on user interests. Table 7 compares reasonably well with the Table 4 results from Kwajalein if one notes that the ranges of ESIp have changed. The cumulative frequency distributions for Eurasian and Kwajalein data also compare reasonably well. The range of ESI_5 greater than 0 in Table 8 is similar to the range from 1 to 2 in Table 5, and the range greater than 2 in Table 8 is most similar to the range from 4 to 5 in Table 5. In both cases, the inclusion of low values of ESI_5 such as between 0 and 2 considerably broadens the frequency distribution with significant percentages of R values equal to 0 (11.9 percent, Table 7) and greater than 2 (15.2 percent, Table 7). These increased percentages are most probably explained by partly cloudy areas for ESI_5. The clear areas have ESI_1 and R equal to zero, while the cloudy areas have high values of R due to low ESI_5 in the denominator of R.

Table 6. The Eleven Stations of the Environmental Definition Program

Station Number	Name	Latitude	Longitude
221130	Murmansk	68°58'N	33°03'E
260630	Leningrad	59°58'N	30°18'E
276120	Moscow	55°58'N	37°25'E
333450	Kiev	50°24'N	30°27'E
339460	Simferopol	45°01'N	33°59'E
282250	Perm	58°01'N	56°18'E
352290	Aktyubinsk	50°20'N	57°13'E
361770	Semipalatinsk	50°21'N	80°15'E
384570	Tashkent	41°16'N	69°16'E
307580	Chita	52°01'N	113°19'E
315100	Blagoveshchensk	50°16'N	127°30'E

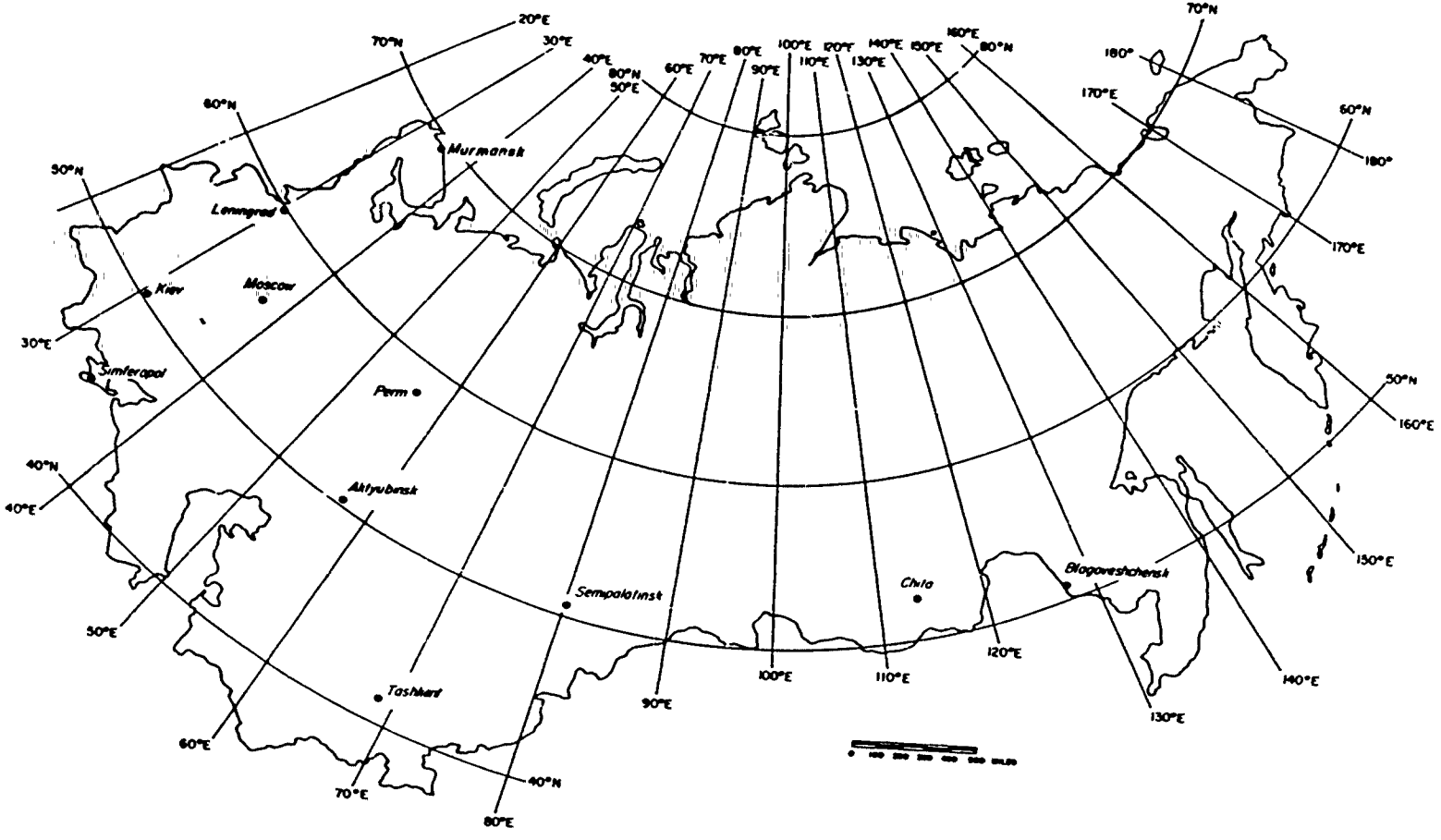

Figure 3. Map Showing the Location of the Eleven Stations Used in the Environmental Definition Program

Table 7. The Frequency Distribution of R for 11 Eurasian Stations

Frequency Distribution (%) Range of ESI_5		
R	> 0	≥ 2
0	11.9	0
> 0-0.2	3.0	0.4
0.2-0.4	3.9	0.7
0.4-0.6	6.4	4.2
0.6-0.8	9.6	12.2
0.8-1.0	14.0	29.1
1.0-1.2	13.2	26.8
1.2-1.4	9.9	15.4
1.4-1.6	6.2	6.2
1.6-1.8	3.9	2.8
1.8-2.0	3.0	1.1
2.0-2.2	2.0	0.6
2.2-2.4	1.6	0.1
2.4-2.6	1.5	0
2.6-2.8	1.1	0.1
2.8-3.0	1.0	0.2
>3.0	8.0	0

Table 8. The Cumulative Frequency Distribution of R for 11 Eurasian Stations

Cumulative Frequency (%) Range of ESI_5		
R	> 0	≥ 2
0	11.9	0
<0.2	14.9	0.4
<0.4	18.8	1.1
<0.6	25.2	5.3
<0.8	34.8	17.5
<1.0	48.8	46.6
<1.2	62.0	73.4
<1.4	71.9	88.8
<1.6	78.1	95.0
<1.8	82.0	97.8
<2.0	85.0	98.9
<2.2	87.0	99.5
<2.4	88.6	99.6
<2.6	90.1	99.6
<2.8	91.2	99.7
<3.0	92.2	99.9

In order to better compare Kwajalein and Eurasian results, the frequency distributions for ESI_5 above 2 were combined for the Kwajalein results in Table 4. Both Kwajalein and Eurasian (11 stations) results are plotted in Figure 4. The two curves are strikingly similar and this observation is unanticipated since the two sources of data are tropical/oceanic for Kwajalein and subarctic/continental for the 11 Eurasian stations.

The similarity in the two distributions is encouraging since it suggests that a single distribution could be conveniently used to estimate what values of fine scale ESIp are expected given an ESIp based on coarse scale satellite data. This single distribution has been estimated by simply combining the frequency distributions of R for ESI_5 over 2 at Kwajalein and the 11 stations and it is given in Table 9. Given an ESI_5 over 2, the distribution of ESI_1 values is found by multiplying each of the categories of R by the ESI_5 value observed.

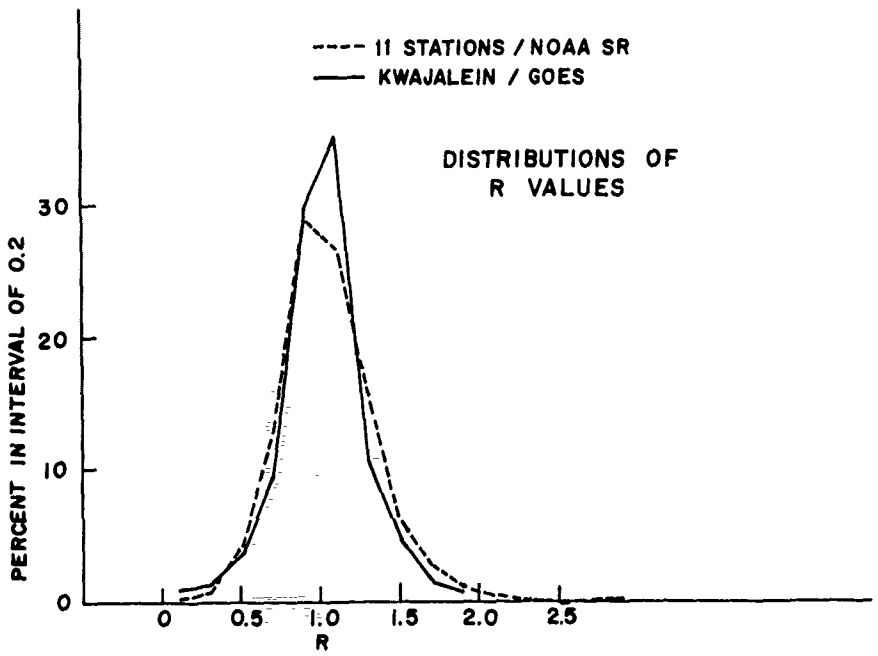

Figure 4. The Distribution of R Values for the Eleven Stations and for Kwajalein When ESI_5 is 2 or Greater

Table 9. The Frequency Distribution of R When ESI_5 is 2 or Greater for Kwajalein Data, Eurasian Station Data, and Combined Data

Frequency Distribution (%)			
R	Kwajalein	Eurasian	Combined
0-0.2	1.0	0.4	0.9
0.2-0.4	1.2	0.7	1.1
0.4-0.6	3.8	4.2	3.9
0.6-0.8	9.6	12.2	10.1
0.8-1.0	29.8	29.1	29.7
1.0-1.2	35.2	26.8	33.5
1.2-1.4	10.6	15.4	11.6
1.4-1.6	4.8	6.2	5.1
1.6-1.8	1.6	2.8	1.9
1.8-2.0	0.4	1.1	0.5
>2.0	2.1	1.0	1.9

Simple inspection of the frequency distribution in Table 9 and Figure 4 suggested that it might be Gaussian. If this were true, a useful alternative to the Table 9 distribution would be a table of the cumulative standardized normal distribution function

$$\phi(u) = \frac{1}{\sqrt{2\pi}} \int_{-\infty}^{u} e^{\frac{-x^2}{2}} dx \qquad (3)$$

along with the standard deviation σ, and the mean $\bar{R}$, of the distribution needed to transform values of R to a standardized variable X in the relation

$$x = \frac{R - \bar{R}}{\sigma} . \qquad (4)$$

In order to see how well the combined frequency distribution could be fit by a Gaussian distribution, the cumulative distribution was plotted on a graph (Figure 5) with an ordinate scale proportional to the standardized variable X. In Figure 5, the ordinate scale is marked with values of the standardized normal distribution function on the left and standard deviations from the mean on the right. The abscissa scale is proportional to R. With these scales, a normal distribution will appear as a straight line plot, but this is not the case for the combined distribution of R. The R distribution is leptokurtic, that is, it differs from a normal distribution by having higher frequencies near the mean and tails of the distribution and lower frequencies in the two regions between the mean and the tails.

Although no single Gaussian curve fits the frequency distribution very well, parts of the distribution can be fit to a better approximation. Figure 6 has the combined frequency distribution plotted along with two Gaussian curves. The dashed curved fits the tails of the distribution for R less than 0.4 or greater than 1.6 while the dotted curve, with nearly the same mean but a lower standard deviation, fits the peak of the distribution for R between 0.8 and 1.2. These Gaussian curves were found by trial and error with the assistance of tables of the cumulative standardized normal distribution function.

2.2.2 COMPARISON OF SATELLITE ESTIMATES

In the original satellite applications,[1] ESIp estimates were presented as exceedance statistics such as Table 10. The percentage of cases for which the ESIp is equal to or greater than a given threshold is tabulated for ESIp thresholds of 1 through 10. The table gives an estimate of the percentage of time a reentry vehicle will experience increasing levels of weather erosion to the extent that the ESIp parameter predicts weather erosion. The percentages are derived from the 847 cases of ESI_5 over Europe and Asia.

16

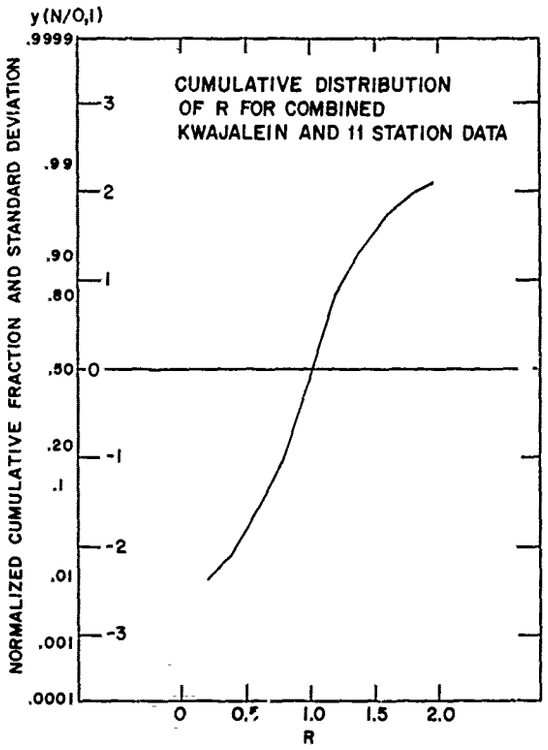

Figure 5. The Cumulative Distribution of R for Combined Kwajalein and Eleven Station Data

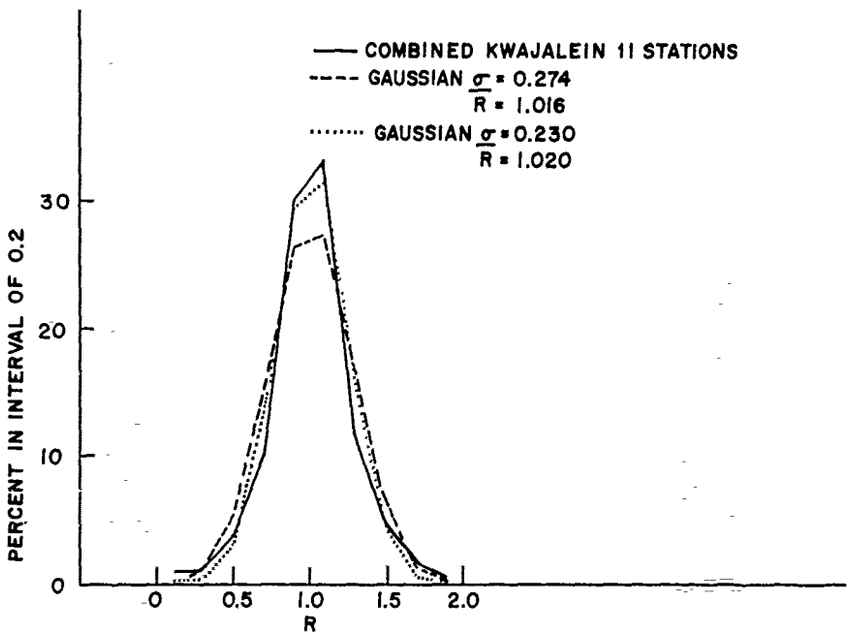

Figure 6. The Combined Distribution of R Values Compared to Two Gaussian Distributions

Table 10. Comparison of Satellite ESI Estimates for 11 Stations During May, July, Oct 1973

Exceeding	ESI_1	ESI_5
1	12.95%	11.69%
2	5.87%	4.01%
3	2.85%	2.24%
4	1.41%	0.71%
5	0.55%	0.24%
6	0.24%	0.12%
7	0.10%	0
8	0.06%	0
9	0.02%	0
10	0.02%	0

In Table 10, the ESI_1 percentages are greater than the ESI_5 percentages for all thresholds. This observation was anticipated in Section 2.1 since the ratio R relating ESI_1 to ESI_5 has average values greater than one. Moreover, the ESI_1 percentages become larger relative to the ESI_5 percentages as the threshold increases so that they are twice as great for thresholds of 4, 5, and 6. For ESI_1, small percentages are found for thresholds 7 through 10 while nothing at all is found for ESI_5. These differences in statistics for ESI_1 and ESI_5 are important since they make the weather threat appear to be greater than the previous study[1] which used ESI_5.

Figure 7 is another comparison of ESIp estimates based on different scales of satellite data. Figure 7 is a picture of two computer plots showing areas with ESIp of 2 or greater. The plot on the upper left of Figure 7 has ESI_5 estimates while the plot on the lower right has ESI_1 estimates for a smaller region. As expected, the areas appear to be larger for the ESI_1 estimates. The ESI_1 estimates show a number of small isolated areas with ESIp of 2 or greater as well as some holes in the larger areas.

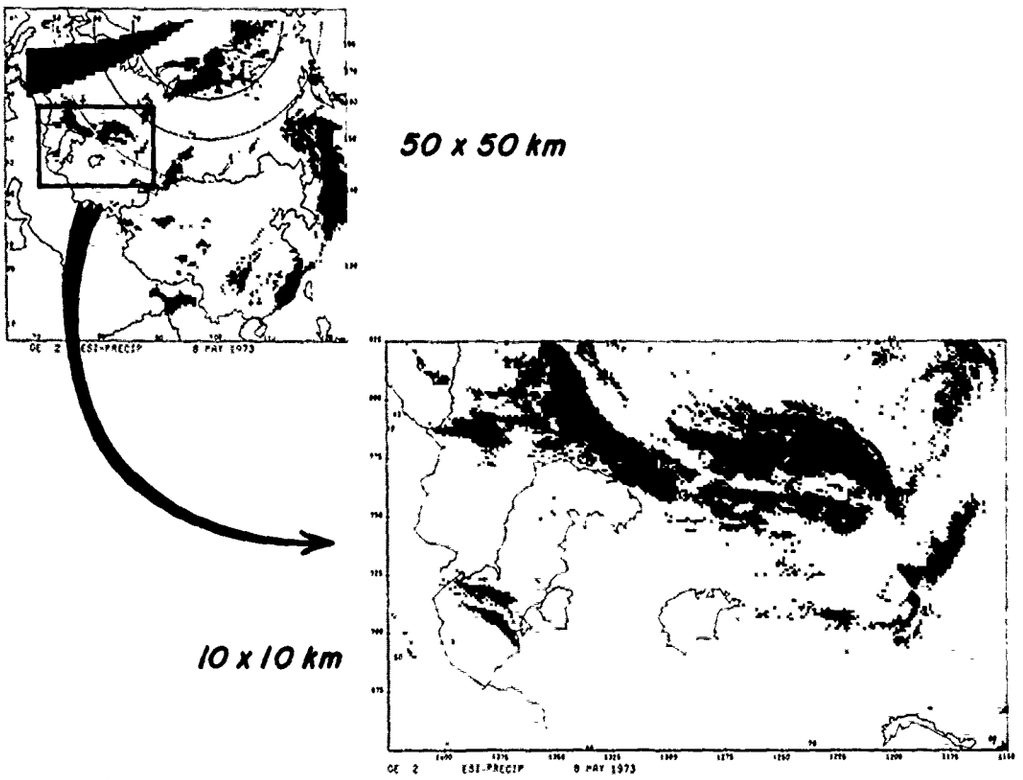

Figure 7. Computer Drawn Plots of Areas With ESIp of 2 or Greater Based on Satellite Data Averaged to 50 X 50 km Resolution and on Unaveraged Data at 10 X 10 km Resolution

2.2.3 COMPARISONS WITH AFGL-2 ESTIMATES

The satellite approach to estimate weather erosion parameters was only one approach out of several used to generate climatologies of weather erosion potential. Since the approaches were different, considerable attention has been given to their comparability.[1,2,3] The satellite estimates of ESIp can be compared to estimates from the AFGL-2 model since AFGL-2 estimates were made for the eleven stations listed in Table 6 at times reasonably close to satellite passes. An initial comparison[1] found that the AFGL-2 model yielded higher percentages of ESIp above 2 than

2. Peirce, R.M., Lenhard, R.W., and Weiss, B.F. (1975) Comparison Study of Models Used to Prescribe Hydrometeor Water Content Values, Part I: Preliminary Results, AFCRL-TR-75-0470, AD A019633.

3. Touart, C.N., and Izumi, Y. (1979) Comparison Study of Models Used to Prescribe Hydrometeor Water Content Values, Part II: USSR Data, AFGL-TR-79-0213, AD A082385.

the satellite model. However, this comparison was made with ESI_5 estimates so the question arises how much of the difference between AFGL-2 and satellite estimates would be explained by the higher percentages observed for the ESI_1 estimates.

The AFGL-2 model was based on a variety of data sources including radiosondes, cloud cover, and precipitation reports from the eleven stations. DMSP satellite pictures and the AF Global Weather Central 3-dimensional nephanalysis (3DNEPH) were available but they played a minor role in the model. First, the various sources of weather data were used to construct time-height cross sections of temperature, moisture, and stability. Next, cloud and precipitation layers were inferred from the cross sections. Finally, ice and liquid water contents were assigned by AFGL meteorologists to establish design profiles of vertical hydrometeor distributions for one year at the eleven stations. The profiles were then converted into various weather erosion estimates including ESIp.

Since AFGL-2 hydrometeor profiles were estimated every 3 hr, the satellite views of the station were within 1.5 hr of an AFGL-2 profile. To improve comparisons, the profiles before and after the satellite pass were converted to ESIp and interpolated to the time of the satellite pass.

Exceedance percentages for AFGL-2 and satellite ESIp values are compared in Figure 8. The satellite values are for ESI_5. The AFGL-2 values are for ESIp estimates adjusted for fractional cloud cover. The hydrometeor density for each cloud and precipitation layer is multiplied by the fraction of horizontal coverage for the layer before the AFGL-2 ESIp is calculated. These ESIp values represent areal averages that can be compared to the satellite estimates which are also areal averages. The satellite ESI_5 percentages are smaller than the AFGL-2 percentages for ESIp of 2 or greater. The satellite ESI_1 percentages (Table 10) are closer to the AFGL-2 percentages but also tend to be smaller than the AFGL-2 percentages for ESIp of 4 or greater. We conclude that the AFGL-2 model provides higher percentages of high ESIp values and that some explanation other than the horizontal scale of satellite estimates is required.

Applications of AFGL-2 data revealed that ESIp could vary substantially for a given hydrometeor profile depending on how the fractional coverage estimates were used. Figure 9 and Table 11 have exceedance percentages for various cloud cover thresholds. The highest percentages are observed for the threshold 1/10 coverage, which counted any cloud or precipitation layer in computing ESIp. This procedure might overestimate ESIp for multilayered cases since the higher clouds might not be directly over the lower clouds. However, it does represent the worst conceivable weather for a vehicle reentering in a partly cloudy area. The lowest percentages are observed for 10/10 coverage, which counted only unbroken layers in computing ESIp. This category represents the best weather for a reentry vehicle. The AFGL-2 exceedance percentages shown in Figure 8, for which hydrometeor

densities were multiplied by fractional coverage, tend to fall between the plots for 4/10 and 6/10 in Figure 9 for ESIp values between 1 and 10. Moreover, the range in Figure 9 between the percentages for 1/10 and 10/10 is greater than the range in Figure 8 between the AFGL-2 percentages and the satellite percentages. In other words, differences in fractional coverage thresholds within the AFGL-2 model are greater than the differences between the AFGL-2 and satellite models. The issue of fractional coverage in the AFGL-2 model is similar in many respects to the issue of horizontal scale variations in satellite estimates.

The 25 ESI_1 values corresponding to each ESI_5 value were ranked from 1st to 25th so that the 1st was the highest ESI_1 and the 25th was the lowest. Exceedance percentages for various ranks are given in Figure 10 and Table 12. The distribution of all ESI_1 values (Table 10) is in the middle of the range of percentages in Figure 10 and is usually close to the percentages for the 10th rank. Similar to the AFGL-2 thresholds of cloud cover, there is a substantial difference between the highest percentages (1st rank) and the lowest percentages. The difference is greater than the difference between AFGL-2 and satellite estimates (Figure 8) for ESIp less than 5.

Comparing Figures 9 and 10, the 1st rank satellite ESI_1 has the highest percentages for ESIp less than 4 while the 1/10 or more AFGL-2 cloud cover has the highest percentages for ESIp greater than 4. The high percentages observed by the satellite for low values of ESIp are assumed to be realistic since noisy records were removed from the satellite data base. Also, the development sample of aircraft data was relatively rich in ESIp values of 1 to 4 so the equation to estimate ESIp is trusted in this range. The satellite is, however, expected to underestimate the percentages of ESIp for values of 8 or greater since Eq. (2) will not predict such high values for the temperatures observed at the high latitudes of the eleven stations during the summer months. For example, using 225°K, the coldest temperature expected in a subarctic summer model temperature profile,[4] and 254, the highest visible count for the NOAA satellites, Eq. (2) provides an ESIp estimate of 7.5. It should be noted that this limit does not apply for mid-latitude or tropical atmospheres since temperatures considerably less than 225°K may be found near the tropopause in these atmospheres.

4. McClatchey, R.A. et al (1972) Optical Properties of the Atmosphere (3rd Edition), AFCRL-TR-72-0497, AD 753075.

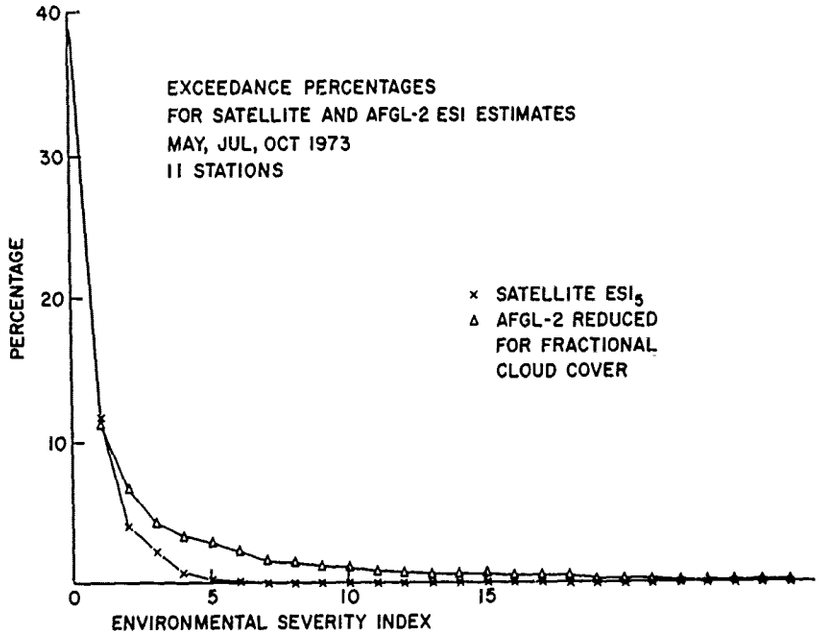

Figure 8. Exceedance Percentages for Satellite and AFGL-2 Estimates of ESIp for the Eleven Stations. Satellite estimates are for ESI_5

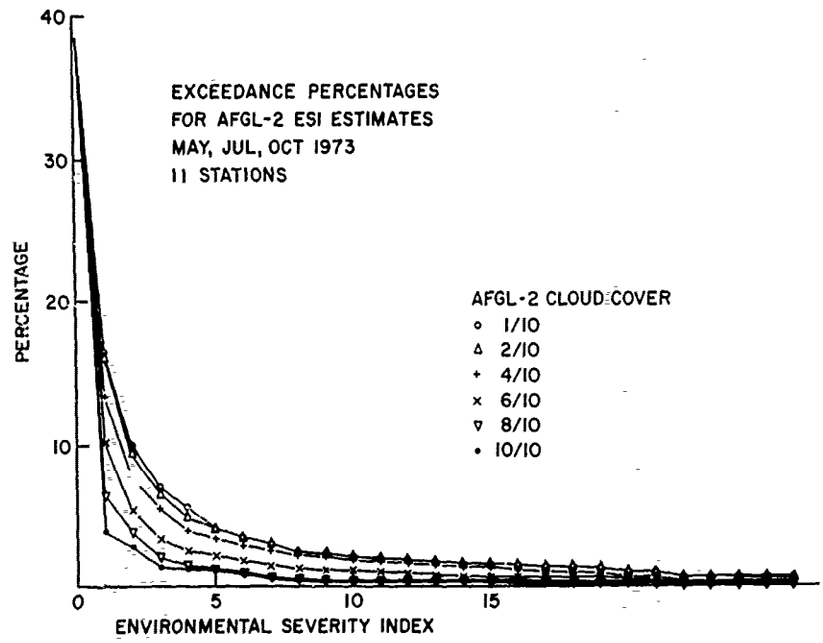

Figure 9. Exceedance Percentages for AFGL-2 ESIp Estimates for Various Cloud Cover Thresholds

Table 11. Exceedance Percentages From AFGL-2 ESIp Estimates for Various Cloud Cover Thresholds From 1/10 to 10/10 and for the Product of Hydrometeor Density and Fractional Cover Described in the Text

ESIp ≥	1/10	2/10	4/10	6/10	8/10	10/10	Density X Fraction
0	100.00	100.00	100.00	100.00	100.00	100.00	100.00
1	16.41	15.94	13.34	10.04	6.38	3.78	11.10
2	9.92	9.21	7.76	5.31	3.78	2.72	6.61
3	6.97	6.49	5.43	3.31	2.01	1.30	4.25
4	5.55	4.84	3.90	2.48	1.42	1.18	3.31
5	4.01	4.01	3.31	2.13	1.18	1.06	2.83
6	3.42	3.42	2.83	1.77	0.94	0.83	2.24
7	2.95	2.95	2.48	1.42	0.59	0.47	1.53
8	2.36	2.36	2.13	1.18	0.47	0.35	1.42
9	2.24	2.24	2.01	1.06	0.35	0.24	1.18
10	2.01	2.01	1.77	1.06	0.35	0.24	1.06
11	1.89	1.89	1.65	0.94	0.35	0.24	0.83
12	1.77	1.77	1.53	0.83	0.35	0.24	0.71
13	1.65	1.65	1.42	0.71	0.35	0.24	0.59
14	1.53	1.53	1.30	0.59	0.35	0.24	0.59
15	1.53	1.53	1.30	0.59	0.35	0.24	0.59
16	1.42	1.42	1.06	0.59	0.35	0.12	0.47
17	1.30	1.30	0.94	0.59	0.24	0.12	0.47
18	1.30	1.30	0.94	0.59	0.24	0.12	0.47
19	1.18	1.18	0.83	0.59	0.24	0.12	0.24
20	0.94	0.94	0.59	0.47	0.24	0.12	0.24
21	0.94	0.94	0.59	0.35	0.12	0.12	0.24
22	0.59	0.59	0.24	0.12	0.00	0.00	0.12
23	0.59	0.59	0.24	0.12	0.00	0.00	0.12
24	0.59	0.59	0.24	0.12	0.00	0.00	0.12
25	0.59	0.47	0.24	0.12	0.00	0.00	0.12
26	0.59	0.47	0.24	0.12	0.00	0.00	0.12
27	0.59	0.47	0.24	0.12	0.00	0.00	0.12
28	0.59	0.47	0.24	0.12	0.00	0.00	0.12
29	0.59	0.47	0.24	0.12	0.00	0.00	0.12
30	0.47	0.35	0.12	0.12	0.00	0.00	0.00

Table 12. Exceedance Percentages for Satellite ESI_1 Estimates for Various Ranks Between 1st and 25th

ESIp ≥	1st	5th	10th	15th	20th	25th
0	100.00	100.00	100.00	100.00	100.00	100.00
1	29.04	18.54	13.11	10.27	7.45	4.07
2	15.58	9.33	5.79	4.13	3.19	1.56
3	8.03	3.90	3.19	2.24	1.18	0.84
4	4.72	2.36	1.30	0.83	0.59	0.12
5	2.48	1.30	0.47	0.12	0.12	0.00
6	1.89	0.59	0.12	0.00	0.00	0.00
7	0.94	0.24	0.00	0.00	0.00	0.00
8	0.47	0.00	0.00	0.00	0.00	0.00
9	0.24	0.00	0.00	0.00	0.00	0.00
10	0.24	0.00	0.00	0.00	0.00	0.00
11	0.24	0.00	0.00	0.00	0.00	0.00
12	0.24	0.00	0.00	0.00	0.00	0.00
13	0.24	0.00	0.00	0.00	0.00	0.00
14	0.12	0.00	0.00	0.00	0.00	0.00
15	0.00	0.00	0.00	0.00	0.00	0.00
16	0.00	0.00	0.00	0.00	0.00	0.00
17	0.00	0.00	0.00	0.00	0.00	0.00
18	0.00	0.00	0.00	0.00	0.00	0.00
19	0.00	0.00	0.00	0.00	0.00	0.00
20	0.00	0.00	0.00	0.00	0.00	0.00
21	0.00	0.00	0.00	0.00	0.00	0.00
22	0.00	0.00	0.00	0.00	0.00	0.00
23	0.00	0.00	0.00	0.00	0.00	0.00
24	0.00	0.00	0.00	0.00	0.00	0.00
25	0.00	0.00	0.00	0.00	0.00	0.00
26	0.00	0.00	0.00	0.00	0.00	0.00
27	0.00	0.00	0.00	0.00	0.00	0.00
28	0.00	0.00	0.00	0.00	0.00	0.00
29	0.00	0.00	0.00	0.00	0.00	0.00
30	0.00	0.00	0.00	0.00	0.00	0.00

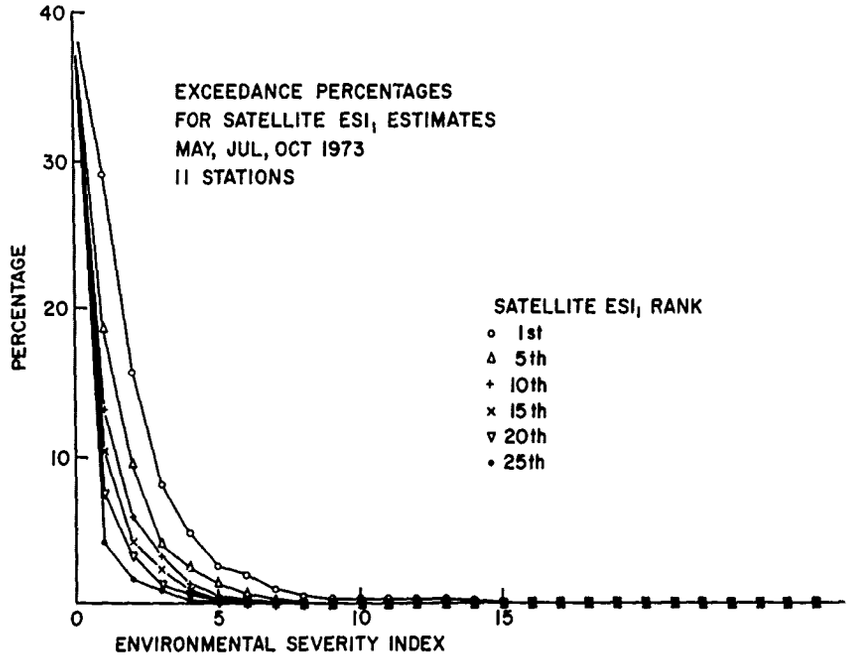

Figure 10. Exceedance Percentages for Satellite ESI_1 Estimates for Various Ranks Between 1st and 25th

3. CONCLUSIONS

ESIp estimates from 5 × 5 spatial averages of satellite data have been compared to estimates from unaveraged data. The comparison shows that the unaveraged data has a 1 percent to 10 percent higher mean ESIp, a factor of 2 or more higher frequency of ESIp values above 3 at high latitudes, and a great range of ESIp variability within the areas for which averages were taken. These results were anticipated since the unaveraged satellite data shows great variability and the equation used to estimate ESIp is nonlinear.

The distribution of ratios relating the ESIp estimates for unaveraged data to estimates from 5 × 5 averages was found to be similar for different satellites and for varied climates such as Kwajalein, Europe, and Asia. The distribution is approximately Gaussian. It could be applied to previous ESIp estimates, which were mostly from averaged satellite data. In future calculations of ESIp, however, one could simply calculate ESIp based on the finest scales of IR and visible data available. Evidence in this report and earlier[1] has been accumulating to favor the use of unaveraged data even though the original aircraft experiments required averaged satellite data. In particular, applications concerned with high ESIp values should use unaveraged satellite data.